Atomistic Analysis of Thermoelectric Properties of Silicon Nanowires

Neophytos Neophytou[#1], Martin Wagner[*2], Hans Kosina[#3]

[#] *Institute for Microelectronics, TU Wien, Gußhausstraße 27-29/E360, A-1040 Wien, Austria*

[1]neophytou@iue.tuwien.ac.at

[3]kosina@iue.tuwien.ac.at

[*]*O' Flexx Technologies, Ratingen, Germany*

[2]m.wagner@o-flexx.com

***Abstract*— The $sp^3d^5s^*$-spin-orbit-coupled tight-binding model and linearized Boltzmann transport theory is applied to calculate the electrical conductivity, the Seebeck coefficient, and the power factor of silicon nanowires (NWs) with diameters *D*<12nm. Using experimentally measured values for the lattice thermal conductivity we estimate the room temperature thermoelectric figure of merit to be *ZT*~1.**

***Keywords*— nanowires, thermoelectrics, power factor, Seebeck, Boltzmann, bandstructure, surface roughness scattering.**

I. Introduction

The ability of a material to convert heat into electricity is measured by the dimensionless figure of merit $ZT=\sigma S^2 T/(k_e+k_l)$, where σ is the electrical conductivity, S is the Seebeck coefficient, and k_e and k_l are the electronic and lattice part of the thermal conductivity, respectively. As a result of suppressed phonon conduction, large *ZT* improvements have been recently reported for nanostructures, compared to the raw materials' values [1, 2, 3, 4]. In silicon, although the bulk material has a ZT_{bulk} ~ 0.01, the *ZT* of silicon NWs was experimentally demonstrated to be *ZT*~0.5. Most of this improvement resulted from suppressed phonon conduction (k_l). It has been suggested, on the other hand, that low dimensionality can be beneficial for increasing the power factor (σS^2) as well, offering an additional *ZT* enhancement [5, 6, 7]. The sharp features in the low-dimensional density of states as a function of energy, *DOS(E)*, can improve *S*, as this quantity is proportional to the energy derivative of *DOS(E)*.

In this work the $sp^3d^5s^*$-spin-orbit-coupled tight-binding model [8, 9, 10, 11] is used to calculate the electronic structure of silicon NWs. Linearized Boltzmann transport theory is applied, including all relevant scattering mechanisms, to calculate the electrical conductivity, the Seebeck coefficient, and the power factor [12, 13]. We examine n-type nanowires of diameters *D*=3nm to *D*=12nm at different doping concentrations, in [100], [110], and [111] transport orientations, as shown in Fig. 1. Using experimental values for the lattice thermal conductivity in NWs, the expected *ZT* value is computed. We find that at room temperature, dimensionality benefits to the power factor due to bandstructure changes alone are possible when the NW diameter is scaled below 7nm. At those dimensions, however, surface roughness scattering strongly degrades the conductivity, and finally the power factor is actually degraded.

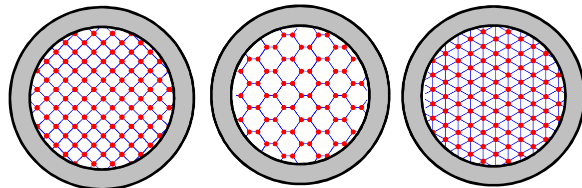

Fig. 1. Cross sections of the nanowires analysed. The [100], [110] and [111] orientations. The nanowire surface is assumed to be passivated.

II. Approach

The NWs' bandstructure is calculated using the 20 orbital spin-orbit-coupled tight-binding model $sp^3d^5s^*$-SO [8, 9, 10, 11]. In this model each atom in the NW is described by 20 orbitals, including spin-orbit-coupling. The NW description is built on the actual zincblende lattice, and each atom is properly accounted for the calculation. It accurately captures the electronic structure and the respective carrier velocities, and inherently includes the effects of quantization and different orientations. The model provides an accurate estimate of the electronic structure, while being computationally affordable. It was extensively used in the calculation of the electronic properties of nanostructures with excellent agreement to experimental observations on various occasions [11].

We examine infinitely long cylindrical n-type NWs, i) of diameters *D*=3nm (ultra scaled) to *D*=12nm (approaching bulk), ii) in [100], [110] and [111] transport orientations, and iii) different doping levels. No relaxation is assumed for the NW surfaces in this study. Figures 2a and 2b show the electronic dispersions of NWs in [100] with diameters *D*=3nm and *D*=12nm respectively. Figures 2c and 2d show the electronic dispersions of NWs in [111] with *D*=3nm and *D*=12nm, respectively. The electronic structure of ultra narrow NWs is sensitive to the diameter and orientation [7, 11]. Differences in the shapes of the dispersions between wires of different orientations and diameters, in the number of subbands, as well as the relative differences in their placement in energy, will result is different electronic properties. It was suggested by bandstructure considerations alone, that low

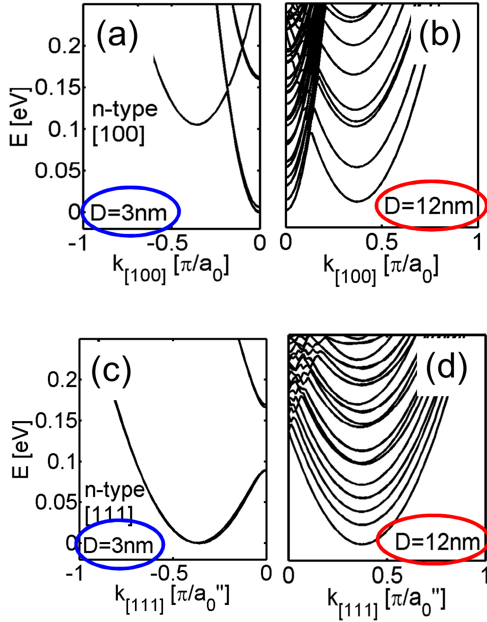

Fig. 2. The electronic structure of n-type NWs for different diameters (*D*) and orientations. (a) *D*=3nm in [100]. (b) *D*=12nm in [100]. (c) *D*=3nm in [111]. (d) *D*=12nm in [111].

dimensionality would benefit the power factor. Indeed, in some cases this is possible. In Fig. 3 we show the power factor versus doping for the [111] n-type NW for different diameters, though under ballistic transport considerations. In this way, only the effect of bandstructure is captured. As the diameter scales from *D*=12nm to *D*=3nm the power factor increases by ~2X. As we will see further on, however, when scattering mechanisms are included this advantage is lost.

To extract the thermoelectric coefficients for each wire considering all relevant scattering mechanisms, linearized Boltzmann theory is applied. The electrical conductivity (σ), the Seebeck coefficient (S), and the electronic part of the thermal conductivity (k_e) are calculated as:

$$\sigma = q_0^{\ 2} \int_{E_c}^{\infty} dE \left(-\frac{\partial f_0}{\partial E} \right) \Xi(E), \tag{1a}$$

$$S = \frac{q_0 k_B}{\sigma} \int_{E_c}^{\infty} dE \left(-\frac{\partial f_0}{\partial E} \right) \Xi(E) \left(\frac{E-\mu}{k_B T} \right), \tag{1b}$$

$$\kappa_0 = k_B^{\ 2} T \int_{E_c}^{\infty} dE \left(-\frac{\partial f_0}{\partial E} \right) \Xi(E) \left(\frac{E-\mu}{k_B T} \right)^2, \tag{1c}$$

$$\kappa_e = \kappa_0 - T\sigma S^2. \tag{1d}$$

The transport distribution $\Xi(E)$ is defined as [12, 13]:

$$\begin{aligned} \Xi(E) &= \sum_{k_x, n} v_n^{\ 2}(k_x)\tau_n(k_x)\delta(E - E_n(k_x)) \\ &= \sum_n v_n^{\ 2}(E)\tau_n(E) g_{1D}^n(E), \end{aligned} \tag{2}$$

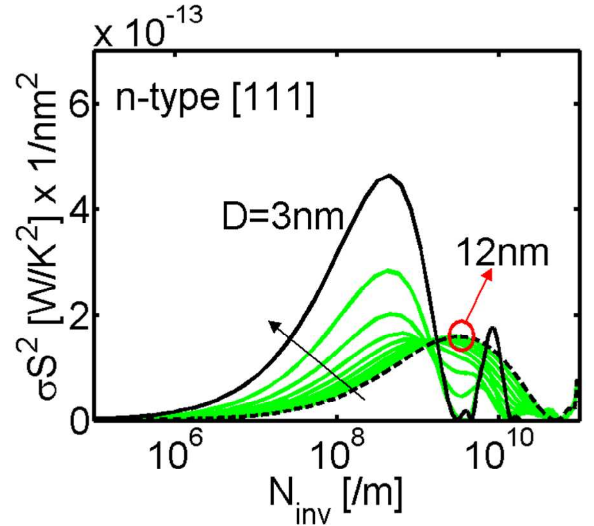

Fig. 3. The power factor versus the doping concentration in n-type [111] NWs with *D*=12nm down to *D*=3nm in decrements of 1nm. Ballistic transport is considered.

where $v_n(E) = \frac{1}{\hbar}\frac{\partial E_n}{\partial k_x}$ is the bandstructure velocity, $\tau_n(k_x)$ is the momentum relaxation time for an electron in the specific k_x-state and subband n, and:

$$g_{1D}^n(E_n) = \frac{1}{2\pi\hbar}\frac{1}{v_n(E)} \tag{3}$$

is the density of states for 1D subbands (per spin). The momentum relaxation rates are extracted using Fermi's Golden rule as:

$$\frac{1}{\tau_n(k_x)} = \sum_{m, k_x'} S_{n,m}(k_x, k_x') \left(1 - \frac{k_x'}{k_x} \right) \tag{4}$$

In this work we used the velocity $v(k_x)$ instead of the momentum k_x in the last parenthesis of Eqn. 4. The two are equivalent in the parabolic band case, but by using the velocity we can also capture curvature variation effects. The phonon scattering rate is given by:

$$\frac{1}{\tau_{Ph.}(E)} = \frac{\pi}{\hbar} \frac{D_{Ph.}^{\ 2}\left(N_\omega + \frac{1}{2} \mp \frac{1}{2} \right)}{\rho\hbar\omega_{Ph.}} \sum_m \frac{1}{A_{nm}} g_{1D}^m(E \pm \hbar\omega_{Ph.}), \tag{5}$$

In the case of elastic ADP scattering, after applying equipartition, the rate is given by:

$$\frac{1}{\tau_{ADP}^n(E)} = \frac{2\pi}{\hbar} \frac{D_{ADP}^{\ 2} k_B T}{\rho \upsilon_s^2} \sum_m \frac{1}{A_{nm}} g_{1D}^m(E), \tag{6}$$

where $D_{ADP} = 9\text{eV}$ is the acoustic phonon deformation potential, ρ is the mass density, υ_s is the speed on sound in Si, N_ω is the number of phonons given by the Bose-Einstein distribution, and $1/A_{nm}$ is the atomistically extracted waveform factor. For inter-valley (IV) scattering we include

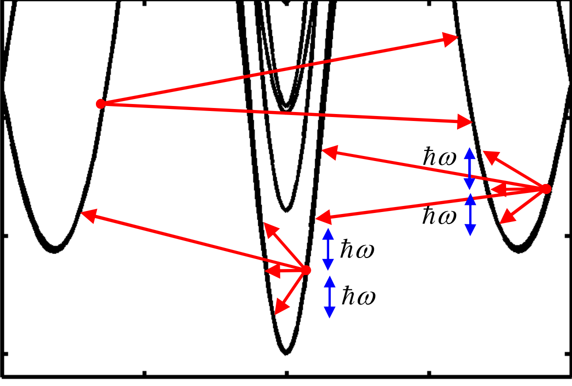

Fig. 4. The electronic structure of the n-type, D=3nm, [110] NW with the scattering mechanisms indicated. Intra-valley elastic and inter-valley inelastic processes are considered (between/within the three valleys), following the bulk silicon scattering selection rules.

all relevant g- and f-processes with parameters given in [15].

For surface roughness scattering SRS, we assume a 1D exponential autocorrelation function for the roughness given by [16]:

$$\langle \delta(\rho)\delta(\rho'-\rho)\rangle = \Delta_{rms}^2 e^{-\sqrt{2}|\rho|/L_C} \quad (7)$$

with Δ_{rms} = 0.48nm and L_C = 1.3nm [17]. The scattering strength is derived from the shift in the band edges with quantization $\frac{\Delta E_c}{\Delta x}$ [18]. Although, this is a simplified way of treatment of SRS (ignores the effect of the wavefunction shape deformation on the interface), it is a valid approximation for ultra scaled channels, where the dominant SRS mechanism is the band edge variation [18, 19, 20]. The transition rate in this case can be derived as [19]:

$$S_{n,m}^{SRS}(k_x,k_x') = \frac{2\pi}{\hbar}\left(\frac{q_0 \Delta E_c}{\Delta x}\right)^2 \left(\frac{2\sqrt{2}\Delta_{rms}{}^2 L_C}{2+\beta^2 L_C{}^2}\right)\delta(E'-E), \quad (8)$$

where $\beta = k_x - k_x'$ and $\delta(E'-E)$ is the delta-function.

For the screened ionized impurities scattering we employ a simple 3D model, in which the potential is:

$$U_S(r) = \frac{q_0{}^2}{4\pi\kappa_s\varepsilon_0 r}e^{-r/L_D}, \quad (9)$$

where the screening length L_D is given by:

$$L_D = \sqrt{\frac{\kappa_s\varepsilon_0 k_B T}{q_0{}^2 n_0}}. \quad (10)$$

Here we have made two approximations: i) We have considered a 3D scattering potential, where in reality 2D solution of the poisson equation should have been employed over the cross section of the NW. This approximation is not valid for low doping, but in that case this scattering mechanism is not important. ii) We have considered a constant wavefunction overlap over the space, which simplifies the integral calculations using the wave form factor integral $1/A_{nm}$. The spatially constant form factor approximation is also more valid at higher concentrations, where impurity scattering becomes important [21]. These approximations significantly reduce the computational and memory cost of the simulation, allowing the treatment of larger NW diameters. Considering a more rigorous treatment of impurity scattering, by removing these assumptions does not change our results for the thermoelectric coefficients significantly. The transition rate is given by:

$$S_{n,m}^{imp.}(k_x,k_x') = \frac{2\pi N_I}{\hbar}\left(\frac{q_0{}^2}{\kappa_s\varepsilon_0 r}\right)^2\left(\frac{1}{1+\beta^2 L_D{}^2}\right)^2 \delta(E'-E), \quad (11)$$

where N_I is the number of impurities in the normalization volume, also considered to be $N_I = n_0$.

We consider bulk phonons, and bulk Si scattering selection rules. Figure 4 shows the electronic structure of a cylindrical NW in the [110] transport orientation. There are three two-fold degenerate valleys in the dispersion relation, one placed at the Γ point, and two placed off-Γ. Elastic and inelastic scattering processes are included (including both f- and g-processes for all six relevant phonon modes in Si), as indicated in Fig. 4. The processes are treated using the bulk Si selection rules. For example, each valley in Fig. 4 is two-fold degenerate, but only intra-valley scattering is allowed, i.e. each valley scatters only within itself. Therefore, inelastic processes are allowed not only between, but also within the Γ and off-Γ valleys of the 1D dispersion.

III. Results

Figure 5 shows the thermoelectric coefficients for the [111] n-type NW for diameters D=12nm and D=3nm versus the electron concentration with all scattering mechanisms considered. We have chosen this particular NW as an example, however, the basic features apply for the rest of the n-type NW orientations as well. Figure 5a shows the conductivity of the two NWs. The conductivity of the smaller diameter is degraded due to stronger phonon scattering originating from the larger form factor (inversely proportional to the NW's area), but more importantly from the effect of SRS, which is particularly strong as the diameter decreases. Figure 5b shows the Seebeck coefficient of the NWs. The Seebeck coefficient at the same 3D electron density is larger for the smaller diameter NWs. This indicates the beneficial effect of dimensionality also shown in Fig. 2. In the case of Fig. 2, however, under ballistic conditions the conductivity is not reduced with diameter. This increase in the Seebeck coefficient is what causes the increase in the power factor (S is scattering independent at first order). Figure 5c shows the power factor which is overall reduced for the smaller diameter NWs. This indicates that the reduction in conductivity dominates over the increase of the Seebeck coefficient.

Although we have used the [111] NW as an example, similar conclusions also apply for NWs in the other transport orientations. Figure 5 shows the ZT values as a function of the electron concentration for the [100] (dash-dot), [110] (dash) and [111] (solid) transport orientation NWs. We show results for D=3nm and D=12nm. To calculate ZT we have used a constant value for the lattice part of the thermal conductivity k_l=2W/mK. This is an experimentally measured value for

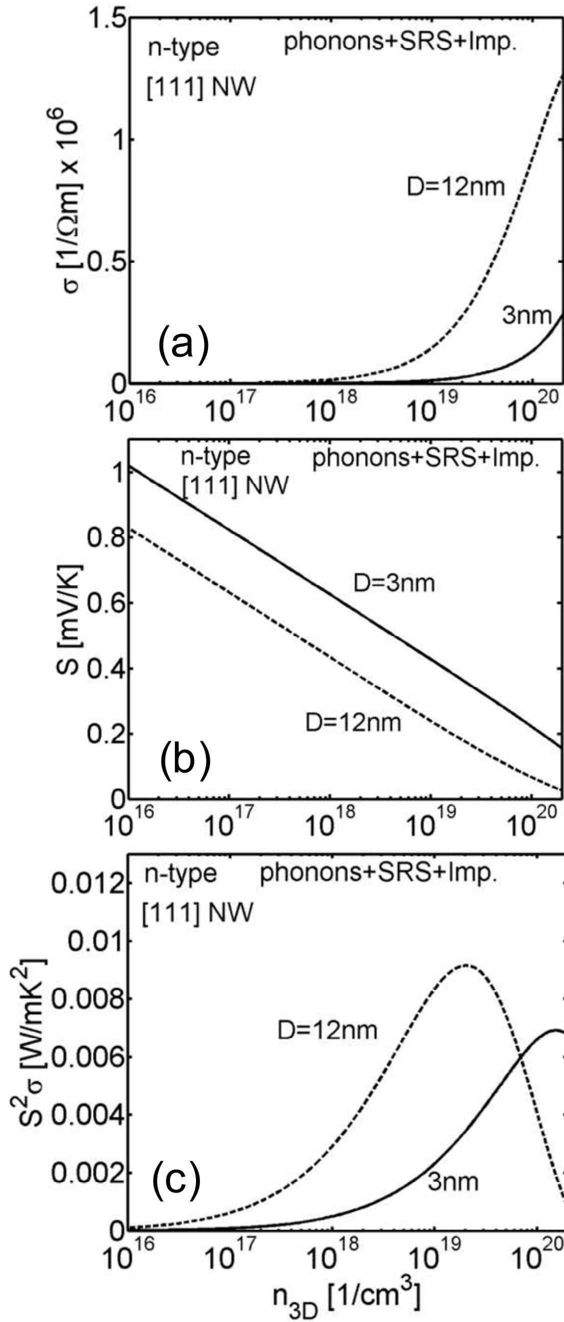

Fig. 5. Thermoelectric coefficients for the [111] NWs with D=3nm (solid) and D=12nm (dash). (b) The electrical conductivity. (b) The Seebeck coefficient. (c) The power factor.

NWs of diameters D~15nm [1, 22, 23]. This value can be even smaller for smaller diameters, as well as orientation-dependent [24], but we use it only to provide an estimate for the expected *ZT*. Our calculated *ZT* values are of the order of *ZT*~1, which is in agreement with other reports, both theoretical [25] and experimental [1, 2]. The *ZT* trends follow the power factor trend, and the performance of the smaller diameter NWs is reduced compared to that of the larger ones. Some orientation dependence is observed, for example the peak of the D=12nm [100] NW is higher than the peaks of the rest. For the smaller diameters the [110] performs somewhat better (at least for concentrations below10^{19}/cm^3). The differences, however, are in general small, and subject to the specific values used for the scattering parameters.

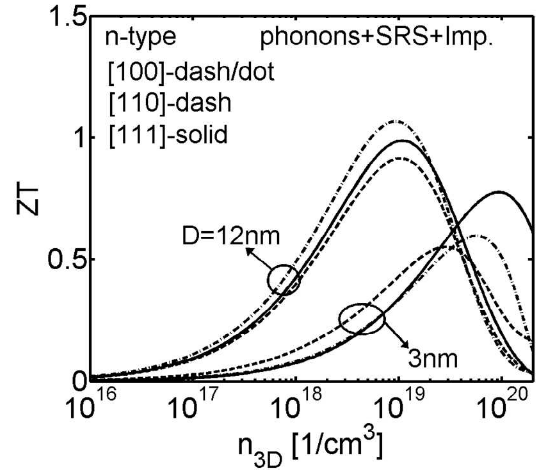

Fig. 6. The *ZT* figure of merit for NWs in the [100], [110], and [111] orientations for diameters D=3nm and D=12nm.

IV. Conclusions

The thermoelectric coefficients (σ, S, σS^2, k_e, ZT) are calculated for n-type silicon NWs in different transport orientations for diameters from D=3nm to D=12nm using the linearized Boltzmann approach. The $sp^3d^5s^*$-SO TB model was used for the electronic structure calculation. Although, under ideal (ballistic) conditions, diameter scaling below 7nm can enhance the power factor of Si NWs by up to 2X [7], enhanced scattering (especially SRS) at those diameter scales weaken this possibility. The reduction in the conductivity is stronger than the increase in the Seebeck coefficient, and the overall power factor and *ZT* are reduced.

Acknowledgment

This work was supported from the Austrian Climate and Energy Fund, contract No. 825467.

References

[1] A. I. Hochbaum, R. Chen, R. D. Delgado, W. Liang, E. C. Garnett, M. Najarian, A. Majumdar, and P. Yang, Nature, vol. 451, pp. 163-168, 2008.

[2] A.I. Boukai, Y. Bunimovich, J. T.-Kheli, J.-K. Yu, W. A. G. III, and J. R. Heath, Nature, vol. 451, pp. 168-171, 2008.

[3] R. Venkatasubramanian, E. Siivola, T. Colpitts, and B. O' Quinn, Nature, vol. 413, pp. 597-602, 2001.

[4] W. Kim, S. L. Singer, A. Majumdar, D. Vashaee, Z. Bian, A. Shakouri, G. Zeng, J. E. Bowers, J. M. O. Zide, and A. C. Gossard, Appl. Phys. Lett., vol. 88, p. 242107, 2006.

[5] L.D. Hicks, and M. S. Dresselhaus, Phys. Rev. B, vol. 47, no. 24, p. 16631, 1993.

[6] M. Dresselhaus, G. Chen, M. Y. Tang, R. Yang, H. Lee, D. Wang, Z. Ren, J.-P. Fleurial, and P. Gagna, Adv. Mater., vol. 19, pp. 1043-1053, 2007.

[7] N. Neophytou, M. Wagner, H. Kosina, and S. Selberherr, Journal of Electronic Materials, vol. 39, no. 9, pp. 1902-1908, 2010.

[8] T. B. Boykin, G. Klimeck, and F. Oyafuso, Phys. Rev. B, vol. 69, no. 11, pp. 115201-115210, 2004.

[9] G. Klimeck, S. Ahmed, B. Hansang, N. Kharche, S. Clark, B. Haley, S. Lee, M. Naumov, H. Ryu, F. Saied, M. Prada, M. Korkusinski, T. B. Boykin, and R. Rahman, IEEE Trans. Electr. Dev., vol. 54, no. 9, pp. 2079-2089, 2007.
[10] G. Klimeck, S. Ahmed, N. Kharche, M. Korkusinski, M. Usman, M. Prada, and T. B. Boykin, IEEE Trans. Electr. Dev., vol. 54, no. 9, pp. 2090-2099, 2007.
[11] N. Neophytou, A. Paul, M. S. Lundstrom and G. Klimeck, IEEE Trans. Electr. Dev., vol. 55, no. 6, pp. 1286-1297, 2008.
[12] G. D. Mahan and J. O. Sofo, Proc. Natl. Acad. Sci. USA, vol. 93, pp. 7436-7439, 1996.
[13] T. J. Scheidemantel, C. A.-Draxl, T. Thonhauser, J. V. Badding, and J. O. Sofo, Phys. Rev. B, vol. 68, p. 125210, 2003.
[14] A. K. Buin, A. Verma, A. Svizhenko, and M. P. Anantram, Nano Lett., vol. 8, no. 2, pp. 760-765, 2008.
[15] M. Lundstrom, “Fundamentals of Carrier Transport,” Cambridge University Press, 2000.
[16] S. M. Goodnick, D. K. Ferry, C. W. Wilmsen, Z. Liliental, D. Fathy, and O. L. Krivanek, Phys. Rev. B, vol. 32, p. 8171, 1985.
[17] S. Jin, M. V. Fischetti, and T. Tang, Jour. Appl. Phys., 102, 83715. 2007.
[18] K. Uchida and S. Takagi, Appl. Phys. Lett., vol. 82, no. 17, pp. 2916-2918.
[19] T. Fang, A. Konar, H. Xing, and D. Jena, Phys. Rev. B, 78, 205403, 2008.
[20] J. Wang, E. Polizzi, A. Ghosh, S. Datta, and M. Lundstrom, Appl. Phys. Lett., 87, 043101, 2005.
[21] G. Fishman, Phys. Rev. B, 34, 4, 2394, 1986.
[22] D. Li, Y. Wu, R. Fan, P. Yang, and A. Majumdar, Appl. Phys. Lett., vol. 83, p. 3186, 2003.
[23] R. Chen, A. I. Hochbaum, P. Murphy, J. Moore, P. Yang, and A. Majumdar, Phys. Rev. Lett., vol. 101, p. 105501, 2008.
[24] T. Markussen, A.-P. Jauho, and M. Brandbyge, Nano Lett., vol. 8, no. 11, pp. 3771-3775, 2008.
[25] T. T.M. Vo, A. J. Williamson, and V. Lordi, Nano Lett., vol. 8, no. 4, pp. 1111-1114, 2008.